Chemical Engineering Science 102 (2013) 324–334

Contents lists available at ScienceDirect

Chemical Engineering Science

journal homepage: www.elsevier.com/locate/ces

CFD simulation of bubbling fluidized bidisperse mixtures: Effect of integration methods and restitution coefficient

C. Tagliaferri [a], L. Mazzei [a,*], P. Lettieri [a], A. Marzocchella [b], G. Olivieri [b], P. Salatino [b]

[a] Department of Chemical Engineering, University College London, Torrington Place, London WCIE 7JE, UK
[b] Dipartimento di Ingegneria Chimica, dei Materiali e della Produzione Industriale, Università degli Studi di Napoli, Federico II, P.le Tecchio, 80125 Napoli, Italy

HIGHLIGHTS

- We investigate numerically the dynamics of a fluidized bed of a binary solid mixture.
- We analyze the role of restitution coefficient and integration methods.
- We compare numerical results with experimental data reported in the literature.
- The value of the restitution coefficient does not affect remarkably the bed dynamics in the cases investigated.
- Spatial discretization methods affect significantly the dynamics, in particular the bubble dynamics.

ARTICLE INFO

Article history:
Received 10 April 2013
Received in revised form
31 July 2013
Accepted 8 August 2013
Available online 16 August 2013

Keywords:
CFD
Fluidized beds
Binary powders
Transient fluidization
Integration schemes

ABSTRACT

In this work we simulated the dynamics of a fluidized bed of a binary solid mixture using the isothermal multi-fluid model of the commercial CFD code Fluent 12. We focused the attention on the role of both restitution coefficient and integration methods on the dynamics of the bed, adopting a mixture of solids assorted in size (with constant density) as case study. We employed two methods of spatial discretization: first-order upwind scheme (FUS) and second-order upwind scheme (SUS). We investigated implicit versus explicit time integration methods as well. The numerical diffusion introduced by the FUS resulted in a low bubble fraction in the bed, in turn reducing solid mixing rates. Simulations carried out adopting the SUS were characterized by a reasonable bubble fraction and associated solid mixing rate. The latter method successfully predicted the transition to fully mixed, uniform fluidization conditions. The value of the restitution coefficient did not significantly affect the results of the simulations, as bubble volume fraction and jetsam concentration profiles did not show any significant change within the interval of restitution coefficient values investigated, with the exception of the nearly ideal value of 0.99.

1. Introduction

The technology of gas–solid fluidized beds is adopted in many industrial processes such as drying, freezing, mixing and sieving, as well as catalytic and thermal processes (Bruni et al., 2002; Reuge et al., 2008). The bed dynamics are key features of fluid bed reactors. Bubbles induce excellent gas–solid contact and high rates of heat and mass transfer. The bed fluid dynamic behavior determines whether powders, which often consist of particles differing in size and/or density, mix or segregate; depending on the bed application, one of these two conditions is desirable. For instance, segregation is important in classifiers where solid particles need to separate (Olivieri et al., 2009), whereas mixing is useful in processes that require intimate gas–solid contact. Understanding and predicting both segregation and mixing phenomena is very important for designing, improving and optimizing industrial plants.

The first studies on these subjects started during the 1970s. Rowe et al. (1972), Gibilaro and Rowe (1974), Rowe and Nienow (1976) and Nienow et al. (1978) investigated the mechanisms of bubble-induced particle mixing and circulation in fluidized beds. They described typical particle patterns in fluidized beds. Particles are carried upwards by both the wake and the drift of bubbles and, by continuity, flow downwards in the bubble-free regions. Particles enter the wake zones at the bottom of the vessel and are entrained towards the bed surface. The splitting of the wakes spreads them throughout the bed and is responsible for particles exchange between wake and emulsion phases and for the drift induced by the bubble flow. Rising along the axis of the bed, the bubbles induce axial mixing as the wakes exchange their solid content with the emulsion phase. Concurrently, as the bubbles ascend, particles from above fall through and around them; also, the smaller and denser particles percolate through the interstices created among the bigger and lighter ones by the bubble motion. These two

* Corresponding author. Tel.: +44 20 7679 4328; fax: +44 20 7383 2348.
E-mail addresses: l.mazzei@ucl.ac.uk, luca.mazzei.a@gmail.com (L. Mazzei).

0009-2509/$ - see front matter © 2013 Elsevier Ltd. All rights reserved.
http://dx.doi.org/10.1016/j.ces.2013.08.015

phenomena counter those previously described, promoting axial segregation. So, mixing and segregation occur simultaneously, and their dynamic equilibrium dictates which one prevails. Accordingly, the specific axial profile of particle concentration through the bed depends on the operating conditions adopted. The particles that sink at the bottom of the bed are known as jetsam, while those that accumulate at the top are known as flotsam.

After the studies of the 1970s, the successive step was to experimentally characterize mixing and segregation of polydisperse mixtures under captive fluid dynamic regimes; an extensive literature is available on this subject. Some authors tried to quantify how mixed or segregated powders are by means of a single parameter, usually referred to as mixing (Wu and Bayens, 1999) or segregation (Goldschmidt et al., 2003) index. Other works investigated additional aspects of the stationary behavior of segregating and mixing powders. Cai et al. (1994) estimated quantitatively bubble sizes in pressurized bed combustors. Wang and Chou (1995) analyzed particle concentration profiles and minimum fluidization velocities of ternary powders of particles differing in size, density and shape. Formisani et al. (2001) analyzed the mixing and segregation tendency of a binary mixture of particles having equal density, while Hoffmann et al. (1993), Olivieri et al. (2004) and Joseph et al. (2007) reported segregation profiles for suspensions of particles differing in size and/or density. Focusing on stationary conditions, these articles did not capture the dynamic behavior of the systems studied. Only few articles, using advanced detection techniques, did so. Tanimoto et al. (1980) investigated the particle behavior at bubble passage. Ekinci et al. (1990) introduced a new technique consisting in measuring temperature profiles for detecting mixing and segregation in fluidized bed combustors, while Goldschmidt et al. (2003) adopted a digital image analysis technique to study bed dynamics and segregation rates.

Even though experimental studies give a deep insight into the behavior of fluidized mixtures, they are highly dependent on the system investigated; therefore, one should couple experimental results with modeling to support the design and optimization of new systems.

The design of fluidized beds has been typically based on experimental correlations. Unfortunately, these correlations lack general validity and cannot support scale-up and optimization of operating conditions (Mazzei et al., 2006). A considerable support to these design issues is provided by the increase of computer power: the dynamic behavior of fluidized powders may now be described by more realistic models (Mazzei, 2011; Mazzei et al., 2012; Mazzei, 2013). Two modeling approaches are available to describe fluid–particle flows: continuum (Euler–Euler) multi-fluid models and discrete (Euler–Lagrange) single-fluid models. Both models describe the fluid phase as a continuum, but the solid phase is treated differently. Discrete models describe the granular phase at particle level and solve the Newtonian equations of motion for all particles, coupling them with the equations of motion for the fluid phase. Conversely, multi-fluid models, firstly introduced by Anderson and Jackson (1967), extend the continuum concept to the solid phases, considering both the solid and fluid phases as interpenetrating continua and solving averaged equations of motion for all phases. Even though several different versions of averaging schemes are available in the literature, all share a common feature: the averaging process generates a closure problem (Lettieri and Mazzei, 2009). Two types of unclosed terms in general arise. The first is related to the linear momentum transport between the phases, while the second to the stress term present in the dynamical equations, which accounts for the transport of momentum, within each phase, owing to particle collisions and velocity fluctuations around the phasic average velocities (Owoyemi et al., 2007). The kinetic theory for granular flows provides closure relationships for the latter undetermined terms, accounting for the energy dissipated during particle collisions by means of restitution coefficients (Gidaspow, 1994; Huilin et al., 2003). Lagrangian models provide a more detailed description of the fluidized bed dynamics but are much more expensive computationally than their Eulerian counterparts; also, they do not usually provide information of direct use to engineers and fluidized bed designers.

Several authors report simulation studies that aim to correctly predict the dynamic behavior of fluid beds. Particularly relevant are those validated experimentally. The following authors analyzed the effect of the values of physical and numerical parameters on the fluid bed dynamics. Employing a discrete model, Hoomans et al. (1998) and Li and Kuipers (2007) studied the effect of restitution and friction coefficients on bubble formation, growth and coalescence. They reported that the bed dynamics can be realistically simulated only when employing non-ideal values of these coefficients. Goldschmidt et al. (2001), Huilin et al. (2003, 2007) and Du et al. (2006) reported that the parameters accounting for the energy dissipated during collisions are of primary importance for bubble formation and segregation patterns, but there is still great need for experiments to determine the values of these parameters. Hulme et al. (2005) analyzed the influence of numerical parameters on bubble properties, whereas Coroneo et al. (2011, 2012) investigated the influence of those parameters on segregation phenomena. Conversely, other authors focused on the models describing the physical phenomena of fluidization. Lettieri et al. (2003) and Cammarata et al. (2003b) investigated alternative Eulerian modeling approaches on the simulation of bubbling fluidized beds. Sun and Battaglia (2006), Taghipour et al. (2005) and Reuge et al. (2008) investigated how different Euler–Euler models affect bubble dynamics, trying to identify the model that best fits experimental data.

This work is part of a wide project aiming to characterize and simulate binary fluidized mixtures. The focus of this contribution is on the fluid dynamic behavior of fluidized suspensions of particles characterized by equal density and different size. The next section reports the main experimental and simulation features of former studies used as reference for this work.

2. Fluid dynamics of fluidized binary mixtures of solids – experimental investigation

This study was based on the experimental investigation of Marzocchella et al. (2000) and Olivieri et al. (2004). We report a summary of their findings in order to contextualize the numerical work conducted in this article. The physical properties of the binary mixture used by these authors and replicated here are reported in Table 1.

A binary powder consisting of jetsam and flotsam solids of same densities was initially completely mixed. The jetsam volume fraction on a fluid-free basis was set at ω_1. Two velocities characterized the fluidization of the binary powder, $u_1(\omega_1)$ and $u_2(\omega_1)$, both function of

Table 1
Material properties.

Property	Silica sand (Flotsam)	Glass beads (Jetsam)
Sauter mean diameter [μm]	125	500
Size [μm]	100–150	400–600
Sphericity [–]	≈1	1
Density [kg/m^3]	2600	2540
Geldart group [–]	B	B
Terminal velocity [m/s]	0.80	4.10
Minimum fluidization velocity [m/s]	0.017	0.220

the initial jetsam composition ω_1. For $u < u_1(\omega_1)$ the bed was fixed and the pressure drop $\Delta p(u)$ through the bed increased linearly. At $u = u_1(\omega_1)$, Δp equaled the weight of the bed per unit cross-sectional area and the transient fluidization phase started. Subsequently, for $u_1(\omega_1) < u < u_2(\omega_1)$, the bed divided in two parts: a defluidized bottom layer rich in jetsam particles and a supernatant, fully fluidized layer rich in flotsam particles. The bottom layer, which was rich in jetsam since segregation started taking place, was at incipient fluidization conditions. Segregation appeared to be due to the *little bubbles* that started appearing in the fluid bed. The height of the bottom layer decreased as the superficial gas velocity increased. For $u > u_2(\omega_1)$, the pressure drop was steadily equal to the bed weight per unit cross-sectional area, and the bed was uniformly mixed because *vigorous bubbling* prevented segregation. Accordingly, $u_1(\omega_1)$ represented the maximum velocity for the fixed bed regime, while $u_2(\omega_1)$ the minimum velocity for the fully fluidized and mixed bed regime.

3. Fluid dynamics of fluidized binary mixtures of solids – simulation study

Mazzei et al. (2010) developed a multi-fluid model for simulating the behavior of binary mixtures in fluidized beds, adopting a first-order spatial discretization scheme. They solved the model using a CFD code, considering a wide range of superficial gas velocities. Testing the model investigated, the authors observed that:

- the value $u_1(\omega_1)$ obtained numerically corresponded to the experimental value measured in Marzocchella et al. (2000);
- for $u_1(\omega_1) < u < u_2(\omega_1)$, the model predicted reasonably well the stationary segregation axial profiles of jetsam concentration;
- the simulations overestimated $u_2(\omega_1)$. The jetsam profile did not show perfect mixing when u equaled the experimental value of $u_2(\omega_1)$, *the simulated bubbling not being sufficiently vigorous to prevent segregation*. For the bed to become fully mixed, the fluid velocity had to exceed significantly the experimental value of $u_2(\omega_1)$.

The model therefore presented some shortcomings, in particular at large superficial fluidization velocities, that is, for $u > u_2(\omega_1)$.

4. Goals of this work and methods adopted to achieve them

Starting from the issues presented, this work moves the study of Mazzei et al. (2010) one step further. In particular, it addresses the following points:

a) Understand why the simulations of Mazzei et al. (2010) correctly predicted the segregation profiles in the transient fluidization regime but failed to do so for the value of the threshold velocity $u_2(\omega_1)$.
b) Determine if the model can correctly predict $u_2(\omega_1)$.
c) Understand how the choices of spatial and temporal discretization schemes affect the results of the numerical simulations.
d) Investigate how the value of the restitution coefficient affects the simulated bed dynamics.

To address these points, we studied the influence of physical properties and numerical options on the simulations, focusing our attention on:

- Spatial discretization schemes: first-order upwind scheme (FUS) and second-order upwind scheme (SUS).
  If the FUS is chosen, cell-face quantities are obtained by assuming that the cell-center values of any field variable represent cell-averages that hold throughout the entire cells; therefore, face quantities are identical to cell quantities, and are set equal to the cell-center values in the upstream cells (relative to the direction of the normal velocity). When the SUS is used, quantities at cell faces are computed with a multidimensional linear reconstruction approach; here the higher-order accuracy is achieved at cell faces through a Taylor series expansion of the cell-centered solution about the cell centroid.
- Temporal discretization schemes: first-order scheme, explicit and implicit.
  An algorithm is explicit if the calculation of a generic variable value at the current time step does not require knowledge of this variable at the present time. Consequently, the variable can be directly computed as it is a function of known values at previous time steps. On the other hand, the implicit method computes the value of a generic variable using the value of the same variable at the current time step; for this reason the equations cannot be solved directly but need successive iterations. If Δt is large, the explicit algorithm could become unstable; the implicit algorithm, conversely, is unconditionally stable with respect to time step size.
- Restitution coefficient.
  This coefficient, denoted as e, characterizes the energy dissipated during particle collisions. Du et al. (2006) defined it as follows:

$$e \equiv \frac{\text{particle speed of separation after collision}}{\text{particle speed of approch before collision}} \tag{1}$$

  Events characterized by equal approach and separation velocities yield $e = 1$, the collision is ideal and no energy is dissipated.
  The lower the value of the restitution coefficient, the more kinetic energy is lost upon collision.

5. Materials

The system studied consisted of a binary mixture of solids having same densities and different sizes. Table 1 reports the properties of the jetsam and flotsam particles, 500 μm and 125 μm in diameter, respectively. The jetsam mass fraction was set at $\omega_1 = 0.5$, and the bed was initially perfectly mixed. To validate the model we referred to the experimental findings of Marzocchella et al. (2000). For the system considered, $u_1(0.5) = 0.02$ m/s and $u_2(0.5) = 0.10$ m/s.

6. Multiphase fluid dynamic model

In a multi-fluid model of binary mixtures, the CFD code solves an averaged equation of motion for the fluid phase and for each solid phase. Table 2 reports the equations of conservation of mass (continuity equations) and linear momentum (dynamical equations) for the fluid phase and for the two particle classes (Savage and Jeffrey, 1981; Lettieri and Mazzei, 2009). Isothermal conditions (for the temperature, not the granular temperatures) were used.

Table 3 reports the equations adopted for the fluid–particle and particle–particle interactions. In this work the former include only the buoyancy and drag forces. Other forces, such as the virtual mass, lift and Faxen forces were considered to be negligible (Owoyemi et al., 2007). The drag force was closed employing the expression developed by Mazzei and Lettieri (2007) and validated in Mazzei and Lettieri (2008). The drag coefficients were computed with the relation of Dallavalle (1948), while the Richardson and Zaki (1954) exponent n was evaluated with the equation of Rowe (1987).

The particle–particle interaction force included only a drag-like contribution and consequently was proportional to the slip velocity between the solid phases. It was expressed with the constitutive equation of Syamlal (1987). The maximum solid compaction ϕ_{max} was specified using the equation of Fedors and Landel (1979).

All the phases were assumed to behave as Newtonian fluids; so, to model the effective stress tensors for the fluid and solid phases, we needed constitutive expressions for the pressure, shear viscosity and dilatational viscosity of every phase. For the solid phases, these variables must be specified for both viscous and plastic regimes (apex v and p, respectively). In the viscous regime, the granular phases are far from the condition of maximum packing and the kinetic theory of dense granular gases holds; here we denote a generic variable $\mathbf{f}_i$ as $\mathbf{f}_i^v$. In the plastic regime, particles experience enduring contacts and approach the maximum packing condition; here $\mathbf{f}_i$ is equal to $\mathbf{f}_i^v+\mathbf{f}_i^p$, where $\mathbf{f}_i^p$ represents the plastic contribution. Constitutive equations for these variables are reported in Table 3. The viscous pressure of the ith particle phase and the viscous dilatational viscosity are expressed using the equations of Lun et al. (1984). The closure for the viscous shear viscosity is that proposed by Gidaspow (1994). Furthermore, the kinetic granular two-fluid based model (refer to Fluent 12 user manual) was chosen to close the plastic variables for the granular phase; in particular, the equation of Schaeffer (1987) was used to express the plastic viscosity of the solids. Table 2 reports also the pseudointernal energy balance equation (Syamlal et al., 1993; Gidaspow, 1994) where the solid viscosities depend on the granular temperatures of the solid phases.

Table 2
Averaged equations of motion and energy for a system of two particle classes.

Averaged equations of motion for binary systems of solids
Continuity equation – fluid phase $\frac{\partial \varepsilon}{\partial t}+\nabla\cdot(\varepsilon\,\boldsymbol{u}_e)=0$
Continuity equation – solid phase i $\frac{\partial \phi_i}{\partial t}+\nabla\cdot(\phi_i\,\boldsymbol{u}_i)=0$
Dynamical equation – fluid phase $\rho_e\left[\frac{\partial}{\partial t}(\varepsilon\,\boldsymbol{u}_e)+\nabla\cdot(\varepsilon\,\boldsymbol{u}_e\,\boldsymbol{u}_e)\right]=\nabla\cdot\boldsymbol{S}_e-n_1\boldsymbol{f}_1-n_2\boldsymbol{f}_2+\varepsilon\,\rho_e\,\boldsymbol{g}$
Dynamical equation – solid phase i $\rho_i\left[\frac{\partial}{\partial t}(\phi_i\,\boldsymbol{u}_i)+\nabla\cdot(\phi_i\,\boldsymbol{u}_i\,\boldsymbol{u}_i)\right]=\nabla\cdot\boldsymbol{S}_i+n_i\boldsymbol{f}_i+n_i\boldsymbol{f}_{ik}+\phi_i\,\rho_i\,\boldsymbol{g}$
Pseudointernal energy balance equation – Solid Phase i $\rho_i\left[\frac{\partial}{\partial t}(\phi_i\,U_i)+\nabla\cdot(\phi_i\,U_i\,\boldsymbol{u}_i)\right]=-\nabla\cdot\boldsymbol{q}_i+\boldsymbol{S}_i:\nabla\boldsymbol{u}_i+G_i^d-S_i^v-S_i^c$
$U_i\equiv(3/2)\Theta_i$ with Θ_i=granular temperature of solid phase i.

6.1. Boundary and initial conditions

The simulated domain, see Table 4, was two-dimensional and the effects of the front and back walls were neglected. The rectangular vessel was 1 m high and 0.12 m large. The bed material occupied 40% of the vessel under rest conditions. The mass fluxes through the walls were set to zero. No-slip conditions were adopted at the walls for both the gas and solid phases. The pressure at the vessel outlet was set to 10^5 Pa. At the bed bottom uniform and constant superficial fluid velocities were specified, equal to 0.10, 0.12 and 0.14 m/s. The values investigated for the restitution coefficient were 0.60, 0.70, 0.80, 0.90 and 0.99.

6.2. Numerical schemes and techniques

The discretization methods investigated were the first-order and the second-order upwind schemes. In most simulations we adopted the implicit time integration scheme. We used the explicit scheme only for restitution coefficients equal to 0.70, 0.80 and 0.90. To integrate the model numerically, we used the commercial CFD package Fluent 12. We used the pressure-based solver, recommended

Table 3
Constitutive equations.

Fluid–particle interaction force

$\boldsymbol{f}_i=\boldsymbol{f}_i^s+\boldsymbol{f}_i^d$

Buoyancy force

$n_i\,\boldsymbol{f}_i^s\equiv\phi_i\,\nabla p_e$

Drag force

$n_i\,\boldsymbol{f}_i^d\equiv\beta_i(\boldsymbol{u}_e-\boldsymbol{u}_i)\beta_i\equiv\frac{3}{4}C_D(\mathrm{Re}_i)\frac{\rho_e|\boldsymbol{u}_e-\boldsymbol{u}_i|\varepsilon\,\phi_i}{d_i}\varepsilon^{-\psi(\varepsilon,\mathrm{Re}_i)}\psi(\varepsilon,\mathrm{Re}_i)\equiv-\frac{\ln\varphi(\varepsilon,\mathrm{Re}_i)}{\ln\varepsilon};\quad\varphi(\varepsilon,\mathrm{Re}_i)\equiv\frac{C_D^*(\varepsilon,\mathrm{Re}_i)}{C_D(\mathrm{Re}_i)}\varepsilon^{2(1-n)}C_D(\mathrm{Re}_i)=(0.63+4.80\mathrm{Re}_i^{-1/2})^2;\quad C_D^*(\mathrm{Re}_i^*)=[0.63+4.80(\mathrm{Re}_i^*)^{-1/2}]^2$

$\mathrm{Re}_i\equiv\frac{\rho_e}{\mu_e}\varepsilon\left|\boldsymbol{u}_e-\boldsymbol{u}_i\right|d_i;\quad\mathrm{Re}_i^*(\varepsilon,\mathrm{Re}_i^*)\equiv\frac{\mathrm{Re}_i}{\varepsilon^n};\quad n(\mathrm{Re}_i^*)=\frac{4.80+2.40\cdot0.175\cdot(\mathrm{Re}_i^*)^{3/4}}{1.00+0.175\cdot(\mathrm{Re}_i^*)^{3/4}}$

Particle–particle interaction forces

$n_i\boldsymbol{f}_{ik}\equiv\zeta_{ik}\,(\boldsymbol{u}_k-\boldsymbol{u}_i);\quad\zeta_{ik}\equiv\frac{3}{4}(1+e_{ik})(1+\frac{\pi}{4}F_{ik})\frac{\rho_i\rho_k\phi_i\phi_k g_{ik}(d_i+d_k)^2}{\rho_i d_i^3+\rho_k d_k^3}\left|\boldsymbol{u}_k-\boldsymbol{u}_i\right|g_i\equiv\frac{d_i}{2}\sum_{k=1}^{2}\frac{\phi_k}{d_k}+\left[1-\left(\frac{\phi}{\phi_{max}}\right)^{1/3}\right]^{-1};\quad g_{ik}\equiv\frac{d_i g_k+d_k g_i}{d_i+d_k}$

$\phi_{max}=\phi_m^i+(1-\xi_{ik})[\phi_m^i+(1-\phi_m^i)\phi_m^k](1-\omega_i)\quad\text{for}\quad\omega_i\geq\frac{\phi_m^i}{\phi_m^i+(1-\phi_m^i)\phi_m^k}$

or otherwise

$\phi_{max}=\phi_m^k+[(\phi_m^i-\phi_m^k)+(1-\xi_{ik})(1-\phi_m^i)\phi_m^k][\phi_m^i+(1-\phi_m^i)\phi_m^k]\frac{\omega_i}{\phi_m^i}\omega_i\equiv\frac{\phi_i}{\phi};\quad\zeta_{ik}\equiv\left(\frac{d_k}{d_i}\right)^{1/2};\quad d_i\geq d_k$

Effective stress – fluid phase

$\boldsymbol{S}_e=-p_e\,\boldsymbol{I}+2\mu_e\,\boldsymbol{D}_e+(\kappa_e-\frac{2}{3}\mu_e)(\mathrm{tr}\,\boldsymbol{D}_e)\boldsymbol{I}\quad\text{with}\quad\boldsymbol{D}_e\equiv\frac{1}{2}(\nabla\mathbf{u}_e+\nabla\mathbf{u}_e^T)$

Fluid considered to be incompressible. μ_e = constant. κ_e = neglected.

Effective stress – solid phase i

$\boldsymbol{S}_i=-p_i\,\boldsymbol{I}+2\,\mu_i\,\boldsymbol{D}_i+(\kappa_i-\frac{2}{3}\mu_i)(\mathrm{tr}\,\boldsymbol{D}_i)\boldsymbol{I}\quad\text{with}\quad\boldsymbol{D}_i\equiv\frac{1}{2}(\nabla\mathbf{u}_i+\nabla\mathbf{u}_i^T)p_i^v=\left[1+2\sum_{k=1}^{2}\left(\frac{d_k}{d_i}\right)^3(1+e_{ik})\phi_k g_{ik}\right]\phi_i\rho_i\Theta_i\quad\text{with}\quad d_{ik}\equiv\frac{d_i+d_k}{2};\quad p_i^p=\text{neglected}.$

$\mu_i^v=\frac{10\rho_i d_i\sqrt{\pi\,\Theta_i}}{96(1+e_i)g_i}\left[1+\frac{4}{5}(1+e_i)\phi_i g_i\right]^2+\frac{4}{5}\phi_i^2\rho_i d_i g_i(1+e_i)\left(\frac{\Theta_i}{\pi}\right)^{1/2}\mu_i^p=\frac{p_i\,\sin\vartheta_i}{2\sqrt{I_2(\boldsymbol{D}_i)}};\quad I_2(\boldsymbol{D}_i)\equiv\frac{1}{2}[(\mathrm{tr}\,\boldsymbol{D}_i)^2-\mathrm{tr}\,\boldsymbol{D}_i^2];\quad\kappa_i^v=\frac{4}{3}\phi_i^2\rho_i g_i(1+e_i)\left(\frac{\Theta_i}{\pi}\right)^2;\quad\kappa_i^p=\text{neglected}.$

Table 4
Simulation settings.

Height of the computational domain	1 m
Width of the computational domain	0.12 m
Initial bed height	0.4 m
Horizontal cell size	0.005 m
Vertical cell size	0.005 m
Number of grid cells in horizontal direction	24
Number of grid cells in vertical direction	200

for low-speed incompressible flows. The code employs the finite-volume method to convert the differential equations into a set of algebraic equations. Pressure and velocity were coupled with the Simultaneous Solution of Non-linearly Coupled Equations (SIMPLE) algorithm. Following the work of Mazzei et al. (2010), which analyzed the accuracy of the results for different time steps, we set the time step to 10^{-3} s. A maximum of 200 iterations was sufficient for the flow variables to converge to the specified threshold of 10^{-5}. Under relaxation factors of 0.20 were adopted for all the variables. The mesh was uniform, with square cells of 5 mm size.

7. Methodology and results

We reported the simulation results in terms of bubble volume fraction δ and of time-resolved profile of jetsam concentration.

Bubble volume fraction. We assessed bubble volume fractions according to the definition reported by Mazzei and Lettieri (2006): a bubble is defined as 'a continuous region of the computational domain comprised solely of cells wherein the solid volume fraction ϕ is less than a threshold value ϕ_{min}'. A higher numerical cut off for bubble boundaries can cause an increase in the bubble volume fraction. As in Mazzei and Lettieri (2006), we set $\phi_{min}=0.30$. We performed a sensitivity analysis setting $\phi_{min}=0.35$ and $\phi_{min}=0.25$; we found that in this range of values the results were unaffected. The procedure for determining the bubble volume fraction was based on the code CFD-post and included the steps reported below. At each time step the procedure computed:

- $N_{0.70}$: the number of cells characterized by a fluid volume fraction greater than 0.70. The number included cells in the freeboard.
- $N_{0.99}$: the number of cells characterized by a fluid volume fraction greater than 0.99. This coincides with the number of cells making up the freeboard.
- N_{bubble}: the number of cells occupied by the bubbles; we obtained this number by subtracting $N_{0.99}$ from $N_{0.70}$.
- N_{bed}: the number of cells occupied by the bed; we obtained this number by subtracting $N_{0.99}$ from the total number of cells present in the domain.

We determined the time-dependent bubble volume fraction using this equation:

$$\delta \equiv \frac{N_{bubble}}{N_{bed}} \equiv \frac{\text{overall bubble volume}}{\text{bed volume}} \tag{2}$$

Axial profiles of jetsam concentration. To determine, for any given superficial fluid velocity u, the stationary profiles of jetsam concentration (fluid-free basis) along the upward vertical axis of the bed, we divided the bed in six horizontal layers of equal height and computed the average values of jetsam volume fraction within each layer. These values were associated with the bed axis levels of the layers upper boundaries. Layer 1 was at the bottom. The procedure is quite similar to the one adopted by Marzocchella et al. (2000): first letting the fluidized bed collapse by cutting off the fluid supply (bed freezing), then dividing the bed in six layers and finally determining the average jetsam concentrations by sieving the powder collected in each layer. Computationally, freezing the bed is unnecessary, for we can easily determine the fluid-free jetsam volume fractions whilst the mixture is fluidized.

7.1. Main phenomenology

In each simulation the system reached stationary conditions within 15 s. As an example, Fig. 1 reports the fluid-free jetsam concentration averaged on six bed layers (see former section) as a function of time. The simulation was conducted setting the gas superficial velocity at 0.10 m/s and the restitution coefficient at 0.70; we adopted the SUS as spatial discretization method and time explicit integration. It is interesting to note that during the first second the jetsam concentration in the bottom and top layers of the bed (layers 1 and 6, respectively) changed linearly with time. The jetsam concentration in the inner layers departed from their initial values (0.50) at about the same time (after about 1.70 s) and the jetsam concentration changed abruptly in the top bed layer. The concentration in each layer fluctuated with time, its time-averaged value gradually approaching a constant value within the first 15 s of simulation.

We can interpret the behavior observed during the first second of simulation by analyzing the CFD snapshots reported in Fig. 2. When the simulation started, two bubbles formed at the bottom of the bed, growing in size while rising through the bed. When the bubbles reached the bed surface, their size was comparable with the vessel diameter, making the jetsam concentration fall abruptly. This mechanism promoted jetsam segregation through the entire bed.

The symmetric behavior reported in Fig. 2 was due to the uniform initial conditions imposed to start the simulation and to the symmetric domain. The initial void fraction was constant everywhere in the bed and the inlet velocity was uniform on the bottom side. Conversely, initial symmetric bubbles are not observed experimentally because the initial void fraction is not constant and the inlet velocity cannot be perfectly uniform across the gas distributor. Numerically, as well as experimentally, one can observe bigger bubbles during the transient condition than during the stationary state. Those big bubbles are due to an instantaneous instability, traveling toward the top of the bed, generated by the sudden opening of the fluid valve.

The bubble growth observed in Fig. 2 is due to the instability development along the bed and to bubble coalescence. Bubbles merge to generate a single bigger bubble. The experimental study of Yates et al. (1994) also documented this phenomenon. Coalescence of small and big bubbles clearly appears in Fig. 2 at $t=0.9$ s and $t=1.5$ s. The edge of small bubbles is making contact with the wake of big bubbles.

The phenomenology of simulations carried out with different operating conditions and integration settings reproduced those

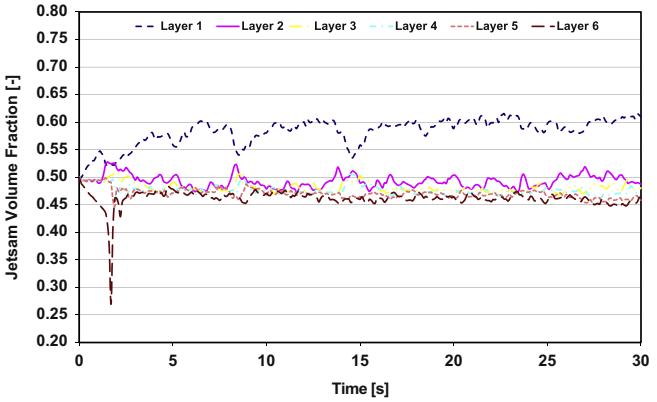

Fig. 1. Time profile of jetsam volume fractions on a fluid-free-basis in the six bed layers for a fluid velocity equal to 0.1 m/s and restitution coefficient equal to 0.7. SUS spatial discretization plus explicit temporal integration.

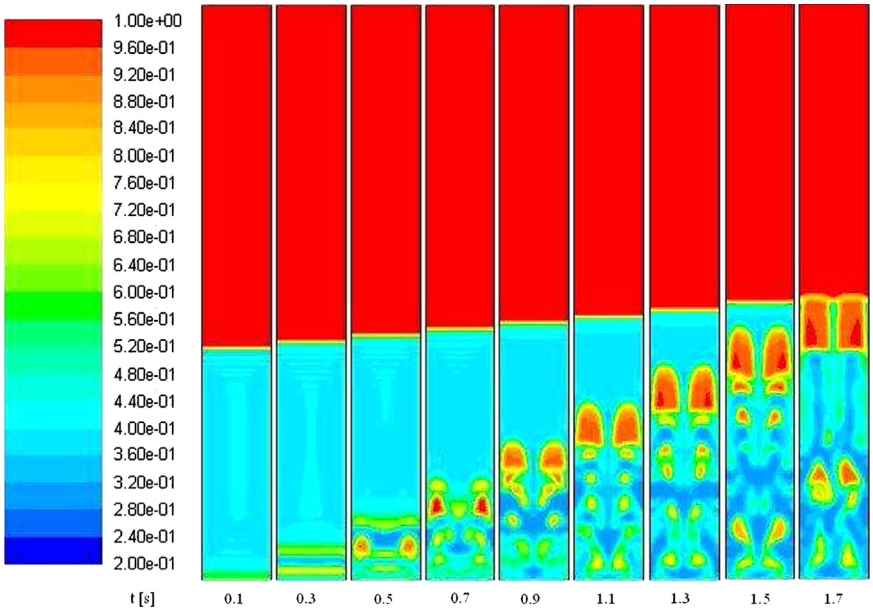

Fig. 2. Transient evolution of bed hydrodynamics for a fluid velocity equal to 0.1 m/s and restitution coefficient equal to 0.7. SUS spatial discretization plus explicit temporal integration.

reported in Figs. 1 and 2. Therefore, each steady state was characterized in terms of time-averaged variables computed according to the following relationship:

$$\langle f \rangle \equiv \frac{1}{t_B - t_A} \int_{t_A}^{t_B} f \, dt \tag{3}$$

where $\langle f \rangle$ denotes the time average of the generic variable f and where the integration limits where set at $t_A = 15$ s and $t_B = 30$ s.

7.2. Mixing and segregation

We ran simulations at velocities $u > u_2(\omega_1) = 0.10$ m/s; the results should show vigorous bubbling and good mixing, as previously mentioned.

Figs. 3–5 report results of simulations carried out with the FUS, while Figs. 6–11 results of simulations carried out with the SUS. We report the jetsam segregation profiles as functions of the bed level normalized with respect to the bed height.

7.2.1. First-order upwind scheme. Implicit time integration

Fig. 3 reports the bubble volume fraction as a function of the restitution coefficient for the three superficial fluid velocities investigated. We employed the FUS and implicit time integration. As the figure shows, the bubble volume fraction is unrealistically low, never exceeding 6%. In this case, at equilibrium, bubbles occupy only a small volume of the bed, which means that there are *few, quite small bubbles*. This is confirmed by Fig. 4 which reports snapshots of the fluid volume fraction for the three values of the superficial fluid velocity at pseudosteady state. The results refer to simulations carried out by setting the restitution coefficient at 0.70, but we found nearly identical results for other values of e. The voidage in the bubbles is far less than unity and bubble size is far smaller than that experimentally observed in fully bubbling beds (Rowe and Nienow, 1976).

Fig. 5 reports the jetsam concentration profiles along the bed axis for different values of the restitution coefficient and for a superficial fluid velocity equal to 0.10 m/s; also in this case, we found results that are qualitatively very similar for other values of u. The profiles clearly show that the bed is segregated, indicating that *the small bubbles present in the bed are not able to induce vigorous mixing*. The scenario

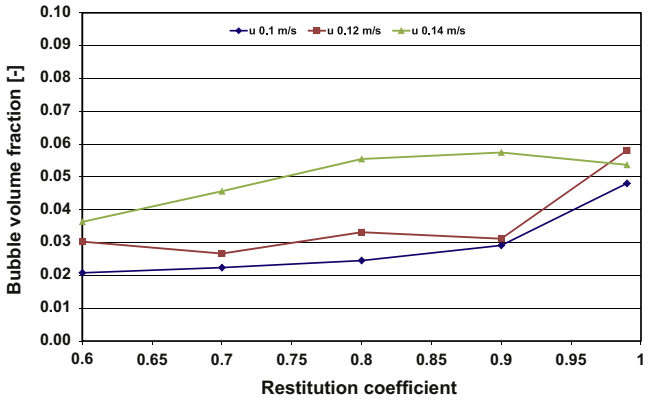

Fig. 3. Stationary profiles of bubble volume fraction as a function of restitution coefficient for different fluid velocities. FUS plus implicit time integration.

did not change remarkably when the restitution coefficient and the superficial gas velocity were varied within the investigated intervals reported in the figures. We can now answer the first point raised in Section 3. We believe that Mazzei et al. (2010) correctly predicted the transient stationary jetsam profiles because the FUS allowed them to reproduce the experimental behavior of transient fluidized powders, since these are indeed characterized by relatively small bubbles.

7.2.2. Second-order upwind scheme. Implicit time integration

Fig. 6 reports the bubble volume fraction as a function of the restitution coefficient for the three superficial fluid velocities investigated. We employed the SUS and implicit time integration. Except for $e = 0.99$, the bubble volume fraction is quite constant with the restitution coefficient and ranges between $\approx 10\%$ for $u = 0.10$ m/s and $\approx 16\%$ for $u = 0.14$ m/s. The simulations carried out at $e = 0.99$ are characterized by bubble volume fractions slightly lower than the values computed for lower values of e. *The values of the bubble volume fraction computed with the SUS are almost one order of magnitude greater than those obtained with the FUS*. Now, at equilibrium, bubbles occupy a larger volume of the fluid bed and are expected to affect more strongly the bulk flow of the suspension. This is confirmed by Fig. 7 which reports snapshots of the fluid volume fraction for the

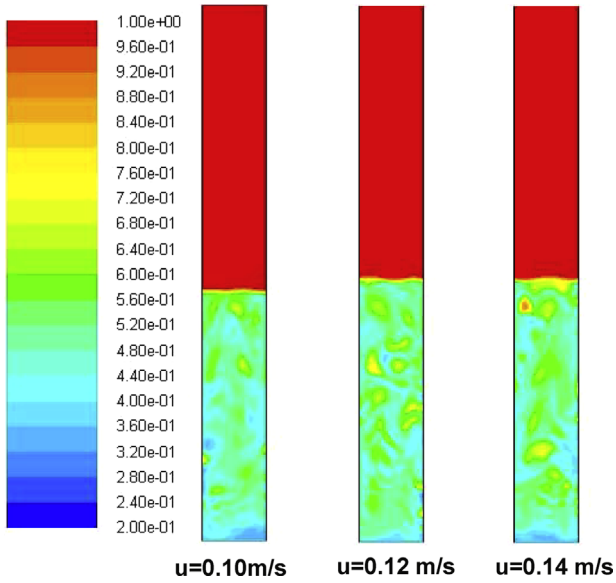

Fig. 4. Spatial profiles of the fluid volume fraction after the bed has reached stationary conditions for superficial fluid velocities equal to 0.10, 0.12 and 0.14 m/s and a restitution coefficient equal to 0.70. FUS plus implicit time integration.

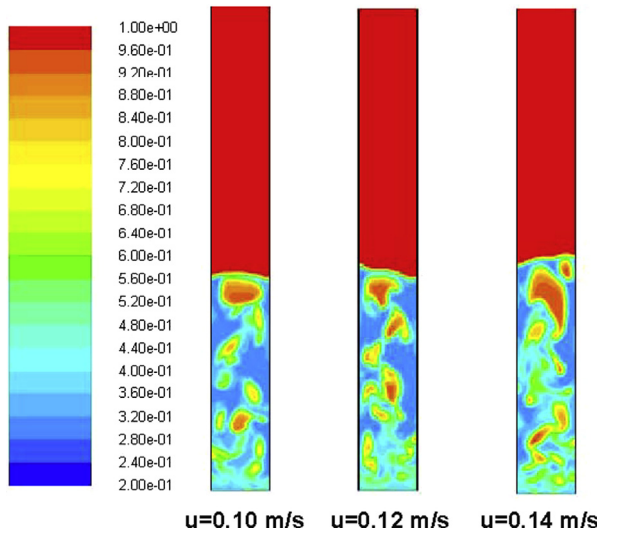

Fig. 7. Spatial profiles of the fluid volume fraction after the bed has reached stationary conditions for superficial fluid velocities equal to 0.10, 0.12 and 0.14 m/s and a restitution coefficient equal to 0.70. SUS plus implicit time integration.

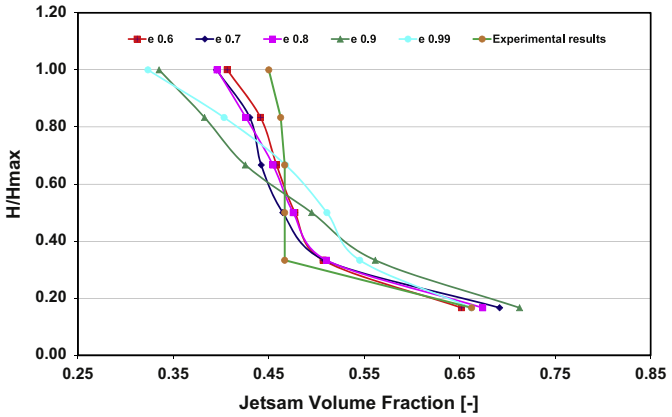

Fig. 5. Stationary axial profiles of average jetsam volume fraction on a fluid-free basis in the six bed layers as a function of restitution coefficient. The superficial fluid velocity is equal to 0.10 m/s. FUS plus implicit time integration. Comparison with experimental data.

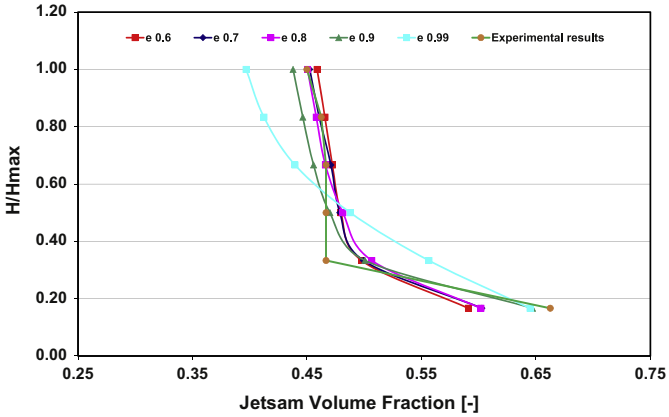

Fig. 8. Stationary axial profiles of average jetsam volume fraction on a fluid-free basis in the six bed layers as a function of restitution coefficient. The superficial fluid velocity is equal to 0.10 m/s. SUS plus implicit time integration. Comparison with experimental data.

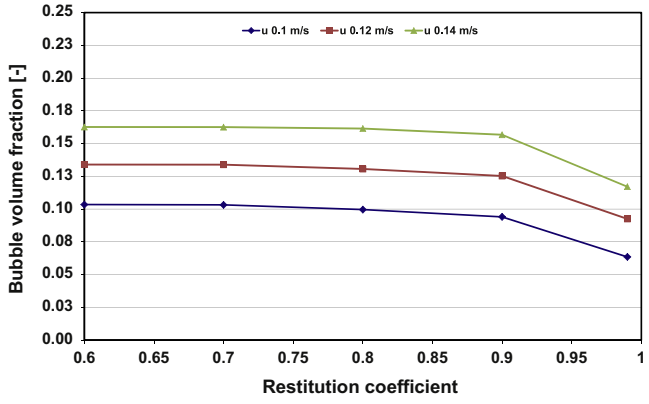

Fig. 6. Stationary profiles of bubble volume fraction as a function of restitution coefficient for different fluid velocities. SUS and implicit time integration.

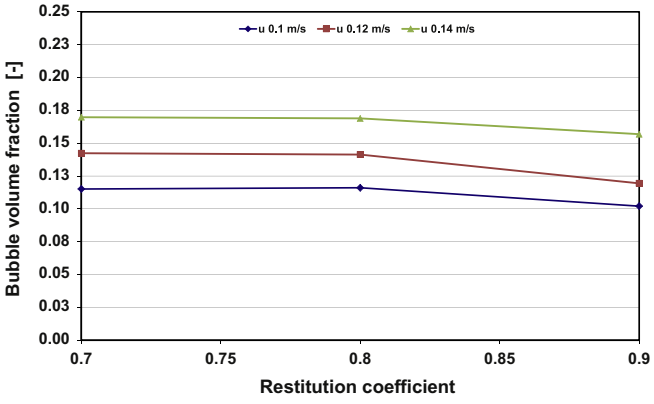

Fig. 9. Stationary profiles of bubble volume fraction as a function of restitution coefficient for different fluid velocities. SUS plus explicit time integration.

three values of the superficial fluid velocity at pseudosteady state. The results refer to simulations carried out by setting the restitution coefficient at 0.70, but do not change remarkably when e is changed within the range investigated. The snapshots show that *the bubbles are larger, with clearly defined boundaries*. In this case, the bubbles occupy a significant part of the bed volume and therefore affect more

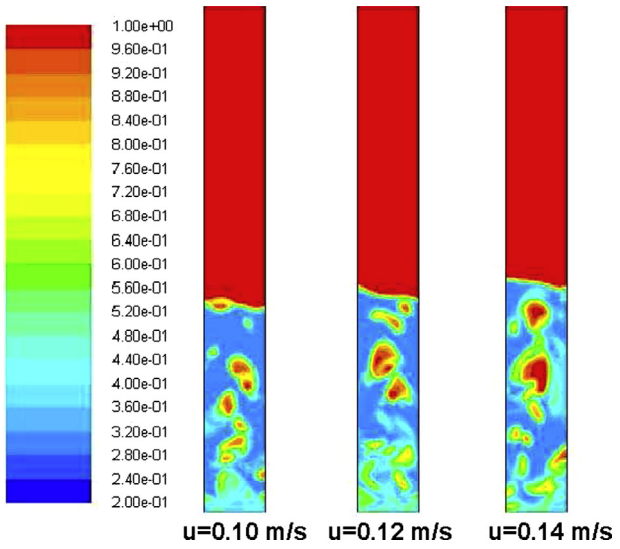

Fig. 10. Spatial profiles of the fluid volume fraction after the bed has reached stationary conditions for superficial fluid velocities equal to 0.10, 0.12 and 0.14 m/s and a restitution coefficient equal to 0.70. SUS plus explicit time integration.

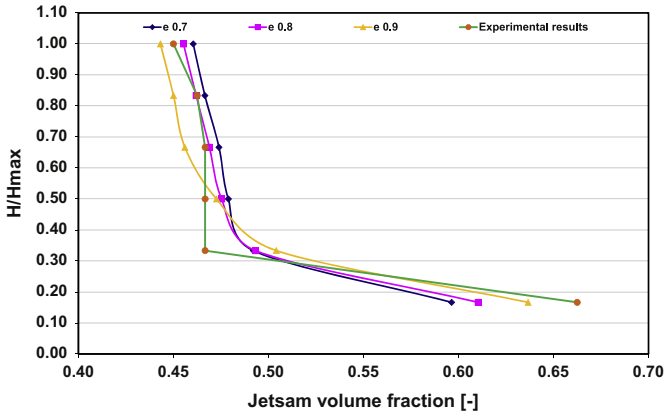

Fig. 11. Stationary axial profiles of average jetsam volume fraction on a fluid-free basis in the six bed layers as a function of restitution coefficient. The superficial fluid velocity is equal to 0.10 m/s. SUS plus explicit time integration. Comparison with experimental data.

strongly the particle dynamics. The void fraction inside the bubbles now approaches unity, and the bubble size agrees with experimental values reported for fully bubbling beds (Rowe and Nienow, 1976).

The bubble flow in the bed makes the jetsam particles migrate towards the upper part of the bed and the flotsam particles sink towards the bed bottom. As a result, particle mixing is strongly enhanced, as evidenced by the axial jetsam concentration profiles reported in Fig. 8. Except for the bottom part of the bed (but this is true also for the experimental profile) and for the case with $e=0.99$, the jetsam concentration is almost constant and equal to the bed average (0.50). At superficial velocities larger than 0.10 m/s, bed turbulence induced by the bubbles enhances mixing. The difference, however, is not very significant, and therefore we do not report additional concentration profiles.

7.2.3. *Second-order upwind scheme. Explicit time integration*

The temporal profiles of the fluid-free jetsam concentration averaged on the six bed layers (profiles similar to those reported in Fig. 1, but here not reported) indicate that in this case the transient phase is slightly longer (for the implicit and explicit time integration the system reaches pseudostationary conditions within 9 and 15 s, respectively). Nevertheless, the time-averaged data referred to the interval 15–30 s is still representative of the pseudosteady-state conditions for the operating conditions investigated.

Figs. 9 and 10 report simulation results obtained using the SUS and explicit time integration. Also in this case we considered the usual three values of the superficial fluid velocity, but, in light of the results previously presented, which did not show a significant influence of this coefficient on the bubble dynamics, we varied the restitution coefficient between 0.70 and 0.90. The reasonable values of the bubble volume fraction obtained when using the SUS with implicit time integration (Fig. 6) are confirmed (also in this case the bubble volume fraction is an order of magnitude higher than the case reported in Section 7.2.1). Large bubbles are seen in Fig. 10, which shows the spatial fluid volume fraction profiles after pseudostationary conditions have been reached. Because the dynamic conditions are similar for all the values of the restitution coefficient studied, we only report the profiles for $e=0.70$. The bubbles induce very effective mixing as one may observe from the axial jetsam concentration profiles reported in Fig. 11.

8. Discussion

As reported in the introduction section, bubbles affect both mixing and segregation of the solids in the bed (Cooper and Coronella, 2005). The two phenomena coexist regardless of the fluidization regime. Depending on which phenomenon predominates under pseudosteady-state conditions, well mixed or segregated beds may establish. The size of the bubbles can identify three different fluid dynamic regimes (Rowe and Nienow, 1976):

- for $u<u_1(\omega_1)$, the bed is fixed. In this case the absence of bubbles prevents the mixing and segregation of the powder.
- for $u_1(\omega_1)<u<u_2(\omega_1)$, the bubbling regime establishes and the jetsam particles segregate at the bed bottom. Since the fluid velocity is not sufficiently high, the jetsam-enriched bed bottom is only incipiently fluidized (thus, bubbles are absent) and bubbles can only mix the solids in the upper fluidized region.
- for $u>u_2(\omega_1)$, vigorous bubbling establishes. The fluid velocity is high enough to fluidize the entire bed. Bubbles promote convective particle transport and solids are fully mixed under pseudosteady-state conditions.

Below we relate our main findings to the work objectives previously stated in Section 4.

a) The choice of the discretization method has a significant effect on the behavior of the simulated bubbling bed. As reported by Mazzei et al. (2010), for $u_1(\omega_1)<u<u_2(\omega_1)$ the FUS correctly predicts the dynamic behavior of the bed, where the small bubbles observed experimentally are matched by the CFD simulations. But for $u>u_2(\omega_1)$, owing to numerical diffusion, the FUS fails to reproduce the vigorous bubbling observed experimentally. This numerical phenomenon is enhanced by this type of discretization scheme, preventing the formation of well-defined bubbles. A bubble represents a discontinuity in the homogeneous phase as the gas volume fraction varies from about 40% in the emulsion phase to about 100% in the void center. Numerical diffusion smooths out the gradients of all variables, in particular of the fluid volume fraction; this explains why the vigorous bubbling observed experimentally is not reproduced numerically: only unrealistically small bubbles are generated in the simulations. For the transient fluidization regime, the FUS

correctly reproduces segregation inasmuch as just small bubbles are present.

b) The model adopted correctly predicts $u_2(\omega_1)$ only if the SUS is used. This is because, owing to lower numerical diffusion, the SUS does not smooth out void fraction gradients and thus correctly simulates the bubbling phenomenon, in particular the vigorous bubbling that establishes at superficial fluid velocities equal to and larger than $u_2(\omega_1)$. This allows to correctly predict the onset of full mixing at pseudostationary conditions.
Figs. 5 and 8 report the comparison between the numerical and the experimental values (Marzocchella et al., 2000) of the averaged jetsam concentration profile for $u=0.10$ m/s. Fig. 5 refers to simulations carried out employing the FUS spatial discretization, while Fig. 8 to the SUS spatial discretization. Both sets of simulations refer to implicit time integration. The figures show that the simulations performed using the FUS fail to correctly predict the bed fluid dynamics when a fully-mixed bed should establish, while the results obtained using the SUS match well the experimental results.
The main difference between the implicit and explicit integration methods is the transient period, this being slightly longer when explicit time integration is adopted (data not reported). Therefore, if one is interested in pseudostationary results, there is no substantial difference between implicit and explicit time integration.

c) The value selected for the restitution coefficient does not affect the numerical results significantly, except for $e=0.99$; this is particularly true when the SUS is adopted, the differences between $e=0.60$ and $e=0.90$ being 3% in the bottom layer of the bed and 23% in the upper layer.
Our findings about the negligible effect of the restitution coefficient are in agreement with those of McKeen and Pugsley (2003) and Zimmermann and Taghipour (2005). These authors studied the effect of the restitution coefficient in the ranges 0.5–0.99 and 0.6–0.975, respectively; they also observed that the restitution coefficient did not change significantly the bubbling bed behavior, the bubble diameter and the bed expansion remaining constant at various values of the restitution coefficient. Furthermore, our results showed that when ideal collisions were modeled the flow behavior was unrealistic, this feature being already reported in Hoomans et al. (1998) and Goldschmidt et al. (2001). These authors studied the effect of the restitution coefficient in the ranges 0.9–1 and 0.73–1, respectively, and stated the importance of adopting non-ideal values of the restitution coefficient to obtain realistic simulation results.

As we have seen, the FUS caused high numerical diffusion. It is possible to lower it by decreasing the size of the cells, but in this case the computational time would increase. Using the SUS has the same effect of reducing the cell size, at least as far as numerical diffusion is concerned, because in both cases (FUS with finer grid and SUS with coarser grid) numerical diffusion is reduced.

9. Conclusions

In this work we have successfully simulated the fluid dynamic behavior of a fluidized bidesperse mixture furthering the work of Mazzei et al. (2010) to correctly reproduce key features of such fluidized systems.

The case study adopted consisted of a bed of particles characterized by equal density and different size. Given the initial average jetsam concentration in the bed (ω_1), experimental findings point out that these systems are characterized by three fluid dynamic regimes (Marzocchella et al., 2000): fixed bed for $u<u_1(\omega_1)$, fully-fluidized and uniformly-mixed bed for $u>u_2(\omega_1)$, and partially-fluidized and segregated transient fluidized bed for $u_1(\omega_1)<u<u_2(\omega_1)$. Mazzei et al. (2010) correctly predicted the value of $u_1(\omega_1)$ and the axial jetsam segregation profiles for $u_1(\omega_1)<u<u_2(\omega_1)$, but overestimated the value of $u_2(\omega_1)$.

The model employed in this work takes into account the effects of restitution coefficient and numerical discretization schemes. The spatial discretization schemes that we investigated were the first-order and the second-order upwind schemes. The time discretization methods were the implicit and explicit schemes. Main conclusions are:

- As reported in Section 3, Mazzei et al. (2010) predicted reasonably well the segregation axial profiles for $u_1(\omega_1)<u<u_2(\omega_1)$, adopting a first-order spatial discretization scheme. In this range bubbles are experimentally small and not vigorous and this is this reason why particles segregate along the bed axis. The numerical diffusion that FUS introduces is not a critical issue in this case because it does not significantly alter the real dynamics of fluidized transient beds.
- The FUS fails to correctly describe the bubble dynamics for values of $u>u_2$ because, in this case, the numerical diffusion becomes a limiting issue for a correct simulation of bed dynamics. The numerical diffusion introduced by the FUS smooths out the solid volume fraction gradients at bubble boundaries, rendering the simulated bubbles unrealistically small. This prevents vigorous mixing and makes the simulated jetsam concentration profiles show unexpected segregation. This explains why Mazzei et al. (2010) obtained numerically fully-mixed fluidization only for $u\approx 0.6$ m/s$\gg u_2$.
- Fully-mixed fluidization is correctly simulated for $u>u_2$ when the SUS is adopted. Large bubbles of realistic size form in this case, inducing significant solid mixing.
- For a given set of operating conditions, if the SUS is used instead of the FUS, the average bubble volume fraction increases by one order of magnitude.
- The selection of explicit versus implicit time integration does not affect the fluid dynamics of the bed under pseudosteady-state conditions. Nevertheless, the system reaches these conditions sooner when implicit integration is selected.
- Except for quasi-ideal collisions ($e=0.99$), the restitution coefficient does not strongly affect jetsam concentration profiles, especially if the SUS discretization is used.

Nomenclature

C_D	particle drag force coefficient
C_D^*	particle drag force coefficient
$\boldsymbol{D}_e$	rate of deformation tensor of fluid (1/s)
$\boldsymbol{D}_i$	rate of deformation tensor of ith particle phase (1/s)
d_i	particle diameter in ith particle phase (m)
d_{ik}	constitutive function (m)
e_{ik}	coefficient of restitution for collisions between particles of ith and kth phases
e	coefficient of restitution for collisions between particles
e_i	coefficient of restitution for collisions between particles of ith phase
f	generic variable (not averaged)
$\langle f\rangle$	generic variable averaged between 15 s and 30 s
$\boldsymbol{f}_i$	force exerted by fluid on ith particle phase per unit particle (kg m/s^2)
$\boldsymbol{f}_i^d$	drag force exerted by fluid on ith particle phase per unit particle (kg m/s^2)
$\boldsymbol{f}_i^s$	buoyancy force exerted by fluid on ith particle phase per unit particle (kg m/s^2)

$\boldsymbol{f}_{ik}$ force exerted by kth particle phase on ith particle phase per unit particle (kg m/s^2)
F_{ik} friction coefficient
$\mathbf{g}$ gravitational acceleration (m/s^2)
g_i radial distribution function in ith particle phase
g_{ik} constitutive function
G_i^d pseudointernal energy source term in ith particle phase (kg/ms^3)
$\mathbf{I}$ identity tensor
n Richardson and Zaki exponent
n_i number density of ith particle phase (1/m^3)
p^* dimensional constant (kg/ms^2)
p_e pressure of fluid (kg/ms^2)
p_i pressure of ith particle phase (kg/ms^2)
p_i^p plastic pressure of ith particle phase (kg/ms^2)
p_i^v viscous pressure of ith particle phase (kg/ms^2)
$\boldsymbol{q}_i$ pseudothermal heat flux in ith particle phase (kg/s^3)
Re_i particle Reynolds number for ith particle phase
Re_i^* particle Reynolds number for ith particle phase
$\boldsymbol{S}_e$ effective stress tensor of fluid (kg/ms^2)
$\boldsymbol{S}_i$ effective stress tensor of ith particle phase (kg/ms^2)
S_i^c pseudointernal energy sink term in ith particle phase (kg/ms^3)
S_i^v pseudointernal energy sink term in ith particle phase (kg/ms^3)
u superficial fluid velocity (m/s)
$\boldsymbol{u}_e$ velocity of fluid (m/s)
$\boldsymbol{u}_i$ velocity of ith particle phase (m/s)
U_i pseudointernal energy of ith particle phase (m^2/s^2)
x axial coordinate (m)
β_i drag force coefficient between fluid and ith particle phase (kg/m^3 s)
δ averaged bubble volume fraction
ε volume fraction of fluid
ε_{min} volume fraction of fluid at maximum packing
κ_e dilatational viscosity of fluid (kg/ms)
κ_i dilatational viscosity of ith particle phase (kg/ms)
κ_i^v dilatational viscosity of ith particle phase in viscous regime (kg/ms)
μ_e shear viscosity of fluid (kg/ms)
μ_i shear viscosity of ith particle phase (kg/ms)
μ_i^p shear viscosity of ith particle phase in plastic regime (kg/ms)
μ_i^v shear viscosity of ith particle phase in viscous regime (kg/ms)
Θ_i granular temperature of ith particle phase (m^2/s^2)
ρ_e mass density of fluid (kg/m^3)
ρ_i mass density of i th particle phase (kg/m^3)
φ_f frictional solid packing
ϕ_i volume fraction of ith particle phase
ϕ_{max} maximum solid packing
ϕ_m^i volume fraction of ith particle phase at maximum solid packing
φ constitutive function
ϑ angle of internal friction
ω_i mass fraction ith particle phase on fluid-free basis
ξ_{ik} constitutive function
ψ constitutive function
ζ_{ik} drag force coefficient between ith and kth particle phases (kg/m^3 s)

References

Anderson, T.B., Jackson, R., 1967. A fluid mechanical description of fluidized beds. Equations of motion. Industrial and Engineering Chemistry Fundamentals 6, 527.

Bruni, G., Solimene, R., Marzocchella, A., Salatino, P., Yates, J.G., Lettieri, P., Fiorentino, M., 2002. Self-segregation of high-volatile fuel particles during devolatilization in a fluidized bed reactor. Powder Technology 128, 11–21.

Cai, P., Schiavetti, M., De Michele, G., Grazzini, G.C., Miccio, M., 1994. Quantitative estimation of bubble size in PFBC. Powder Technology 80, 99–109.

Cammarata, L., Lettieri, P., Micale, G.D.M., Colman, D., 2003b. 2D and 3D CFD simulations of bubbling fluidized beds using Eulerian–Eulerian models. International Journal of Chemical Reactor Engineering 1, A48.

Cooper, S., Coronella, C.J., 2005. CFD simulations of particle mixing in a binary fluidized bed. Powder Technology 151 (1–3), 27–36.

Coroneo, M., Mazzei, L., Lettieri, P., Paglianti, A., Montante, G., 2011. CFD prediction of segregating fluidized bidisperse mixtures of particles differing in size and density in gas–solid fluidized beds. Chemical Engineering Science 66 (11), 2317–2327.

Coroneo, M., Mazzei, L., Lettieri, P., Montante, G., Paglianti, A., 2012. Eulerian–Eulerian simulations of segregating binary gas–solid fluidized beds. International Journal of Nonlinear Sciences and Numerical Simulation 13 (6), 375–382.

Dallavalle, J.M., 1948. Micrometrics. Pitman, New York.

Du, W., Bai, X., Xu, J., Wei, W., 2006. Computation fluid dynamics (CFD) modeling of spouted bed: influence of friction stress, maximum packing limit and coefficient of restitution of particles. Chemical Engineering Science 61 (14), 4558–4570.

Ekinci, E., Atakul, H., Tolay, M., 1990. Detection of segregation tendencies in a fluidized be using temperature profiles. Powder Technology 61, 185–192.

Fedors, R.F., Landel, R.F., 1979. An empirical method of estimating the void fraction in mixtures of uniform particles of different size. Powder Technology 23, 225.

Formisani, B., De Cristoforo, G., Giramonte, R., 2001. A fundamental approach to the phenomenology of fluidisation of size segregating binary mixtures of solids. Chemical Engineering Science 56, 109.

Gibilaro, L.G., Rowe, P.N., 1974. A model for a segregating gas fluidized bed. Chemical Engineering Science 29, 1403.

Gidaspow, D., 1994. Multiphase Flow and Fluidization. Academic Press, London.

Goldschmidt, M.J.V., Kuipers, J.A.M., Van Swaaij, W.P., 2001. Hydrodynamic modelling of dense gas fluidised beds using the kinetic theory of granular flow: effect of coefficient of restitution on bed dynamics. Chemical Engineering Science 56 (2), 571–578.

Goldschmidt, M.J.V., Link, J.M., Mellema, S., Kuipers, J.A.M., 2003. Digital image analysis measurements of bed expansion and segregation dynamics in dense gas-fluidised beds. Powder Technology 138, 135–159.

Hoffmann, A.C., Janssen, L.P.B.M., Prins, J., 1993. Particle segregation in fluidized binary mixtures. Chemical Engineering Science 48, 1583–1594.

Hoomans, B.P.B., Kuipers, J.A.M., Van Swaaij, W.P.M., 1998. The influence of particle properties on pressure signals in dense gas-fuidised beds: a computer simulation study. World Congress on Particle Technology 3.

Huilin, L., Yurong, H., Gidaspow, D., 2003. Hydrodynamic modelling of binary mixture in a gas bubbling fluidized bed using the kinetic theory of granular flow. Chemical Engineering Science 58 (7), 1197–1205.

Huilin, L., Yunhua, Z., Ding, J., Gidaspow, D., Wei, L., 2007. Investigation of mixing/segregation of mixture particles in gas–solid fluidized beds. Chemical Engineering Science 62, 301.

Hulme, I., Clavelle, E., Van der Lee, L., Kantzas, A., 2005. CFD modeling and validation of bubble properties for a bubbling fluidized bed. Industrial and Engineering Chemistry Research 44 (12), 4254–4266, http://dx.doi.org/10.1021/ie049837j.

Joseph, G.G., Leboreiro, J., Hrenya, C.M., Stevens, A.R., 2007. Experimental segregation profiles in bubbling gas-fluidized beds. AIChE Journal 53, 2804–2813.

Lettieri, P., Cammarata, L., Micale, G.D.M., Yates, J.G., 2003. CFD simulations of gas fluidized beds using alternative Eulerian–Eulerian modelling approach. International Journal of Chemical Reactor Engineering 1, A5.

Lettieri, P., Mazzei, L., 2009. Challenges and issues on the CFD modeling of fluidized beds: a review. Journal of Computational Multiphase Flows 1, 83.

Li, J., Kuipers, J.A.M., 2007. Effect of competition between particle–particle and gas–particle interactions on flow patterns in dense gas-fluidized beds. Chemical Engineering Science 62 (13), 3429–3442.

Lun, C.K.K., Savage, S.B., Jeffrey, D.J., Chepurniy, N., 1984. Kinetic theories for granular flow: inelastic particles in Couette flow and slightly inelastic particles in a general flow field. Journal of Fluid Mechanics 140, 223.

Marzocchella, A., Salatino, P., Di Pastena, V., Lirer, L., 2000. Transient fluidization and segregation of binary mixture of particles. AIChE Journal 46, 2175.

Mazzei, L., 2011. Limitations of quadrature-based moment methods for modeling inhomogeneous polydisperse fluidized powders. Chemical Engineering Science 66, 3628.

Mazzei, L., 2013. Segregation dynamics of dense polydisperse fluidized suspensions modeled using a novel formulation of the direct quadrature method of moments. Chemical Engineering Science 101, 565.

Mazzei, L., Casillo, A., Lettieri, P., Salatino, P., 2010. CFD simulations of segregating fluidized bidisperse mixtures of particles differing in size. Chemical Engineering Journal 156, 432–445.

Mazzei, L., Lettieri, P., 2006. A numerical algorithm for the analysis of the bubble dynamics in two-dimensional fluidized beds simulated by means of CFD multiphase-flow codes. International Journal of Chemical Reactor Engineering 4 (Article A26).

Mazzei, L., Lettieri, P., Elson, T., Colman, D., 2006. A revised mono-dimensional particle bed model for fluidized beds. Chemical Engineering Science 61, 1958.

Mazzei, L., Lettieri, P., 2007. A drag force closure for uniformly-dispersed fluidized suspensions. Chemical Engineering Science 62, 6129.

Mazzei, L., Lettieri, P., 2008. CFD simulations of expanding/contracting homogeneous fluidized beds and their transition to bubbling. Chemical Engineering Science 63 (24), 5831–5847.
Mazzei, L., Marchisio, D.L., Lettieri, P., 2012. New quadrature-based moment method for the mixing of inert polydisperse fluidized powders in commercial CFD codes. AIChE Journal 58, 3054–3069.
McKeen, T., Pugsley, T., 2003. Simulation and experimental validation of a freely bubbling bed of FCC catalyst. Powder Technology 129, 139–152.
Nienow, W., Rowe, P.N., Cheung, L.Y.-L., 1978. A quantitative analysis of the mixing of two segregating powders of different density in a gas-fluidised bed. Powder Technology 20, 89–97.
Olivieri, G., Marzocchella, A., Salatino, P., 2004. Segregation of fluidized binary mixtures of granular solids. AIChE Journal 50, 3095.
Olivieri, G., Marzocchella, A., Salatino, P., 2009. A fluid-bed classifier of polydisperse granular solids. Journal of Taiwan Institute of Chemical Engineers 40, 638–644.
Owoyemi, O., Mazzei, L., Lettieri, P., 2007. CFD modeling of binary-fluidized suspensions and investigation of role of particle–particle drag on mixing and segregation. AIChE Journal 53, 1924.
Reuge, N., Cadoret, L., Coufort, C., Pannala, S., Syamlal, M., Caussat, B., 2008. Multifluid Eulerian modeling of dense gas–solids fluidized bed hydrodynamics: influence of the dissipation parameters. Chemical Engineering Science 6, 22.
Richardson, J.F., Zaki, W.N., 1954. Sedimentation and fluidization: Part I. Transactions of the Institution of Chemical Engineers 32, 35.
Rowe, P.N., Nienow, A.W., Agbim, A.J., 1972. The mechanism by which particles segregate in gas fluidised beds-binary systems of near-spherical particles. Transactions of the Institution of Chemical Engineers 50, 310–323.
Rowe, P.N., Nienow, A.W., 1976. Particle mixing and segregation in gas fluidized beds. A review. Powder Technology 15, 141–147.
Rowe, P.N., 1987. A convenient empirical equation for estimation of the Richardson and Zaki exponent. Chemical Engineering Science 42, 2795.
Savage, S.B., Jeffrey, D.J., 1981. The stress tensor in a granular flow at high shear rates. Journal of Fluid Mechanics 110, 255–272.
Schaeffer, D.G., 1987. Instability in the evolution equations describing incompressible granular flow. Journal of Difference Equations 66, 19.
Syamlal, M., 1987. The Particle–Particle Drag Term in a Multiparticle Model of Fluidization. National Technical Information Service, OE/MC/21353–2373, NTIS/DE87006500.
Syamlal, M., Rogers, W.A., O'Brien, T.J., 1993. MFIX Documentation and Theory Guide. DOE/METC94/1004, NTIS/DE94000087. Available from: ⟨http://www.mfix.org⟩.
Sun, J., Battaglia, F., 2006. Hydrodynamic modeling of particle rotation for segregation in bubbling gas-fluidized beds. Chemical Engineering Science 61, 1470–1479.
Taghipour, F., Ellis, N., Wong, C., 2005. Experimental and computational study of gas–solid fluidized bed hydrodynamics. Chemical Engineering Science 60 (24), 6857Y–6867Y.
Tanimoto, H., Chiba, S.H., Kobayashi, H., 1980. Mechanism of solid segregation in gas fluidised beds. Fluidization, 381–388.
Wang, R.C., Chou, C.C., 1995. Particle mixing/segregation in gas–solid fluidized bed of ternary mixtures. Canadian Journal of Chemical Engineering 73, 793–799.
Wu, S.Y., Bayens, J., 1999. Segregation by size difference in gas fluidized beds. Powder Technology 103, 175–181.
Yates, J.G., Cheesman, D., Sergeev, Y.A., 1994. Experimental observations of voidage distribution around bubbles in a fluidized bed. Chemical Engineering Science 49 (12), 1885–1895.
Zimmermann, S., Taghipour, F., 2005. CFD modeling of the hydrodynamics and reaction kinetics of FCC fluidized-bed reactors. Industrial and Engineering Chemistry Research 44, 9818–9827.